Lamellarity and size distributions in mixed DPPC/amphiphilic poly(2-oxazoline) gradient copolymer vesicles and their temperature response

Aristeidis Papagiannopoulos[*,1], Natassa Pippa[1,2], Costas Demetzos[2], Stergios Pispas[1] and Aurel Radulescu[3]

[1]Theoretical and Physical Chemistry Institute, National Hellenic Research Foundation, 48 Vassileos Constantinou Avenue, 11635 Athens, Greece.

[2]Department of Pharmaceutical Technology, Faculty of Pharmacy, Panepistimioupolis Zografou 15771, National and Kapodistrian University of Athens, Athens, Greece.

[3]Jülich Centre for Neutron Science JCNS Forschungszentrum Jülich GmbH, Outstation at Heinz Maier-Leibnitz Zentrum (MLZ), Lichtenbergstraße 1, 85747 Garching, Germany.

Email: apapagiannopoulos@eie.gr

Abstract

Mixed liposomes of dipalmitoylphosphatidylcholine (DPPC) and gradient (pseudodiblock) poly(2-methyl-2-oxazoline)-grad-poly(2-phenyl-2-oxazoline) (MPOx) copolymers are investigated by small angle neutron scattering (SANS). All experimental data, from different phospholipid-copolymer compositions, concentrations and temperatures are fitted with one model. This model allows the determination of the separate contributions from vesicular populations of different lamellarity and size. MPOx copolymers are proved to modify both the size and lamellarity of DPPC liposomes. The gradient copolymer with higher hydrophilic content induces shrinkage of the uni- and bi-lamellar DPPC vesicles. The copolymer with lower hydrophilic content causes dramatic changes on the lamellarity of DPPC vesicles by the formation of hexa-lamellar vesicles. The tendency of multi-lamellar vesicles to transform into uni-lamellar ones as temperature increases is more

pronounced in the presence of the copolymers. These findings may have direct implications on the drug loading and release properties of liposomes and their interactions with cells.

Keywords: small angle neutron scattering; liposomes; DPPC; poly(2-oxazoline); lamellarity

1. Introduction

Liposomes have high biocompatibility and low toxicity and therefore are attractive as carriers of genetic material, drugs and enzymes [1, 2]. Lamellarity, i.e. the number of lipid bilayers in a vesicle, together with size, is a crucial parameter as it affects encapsulation efficiency, release kinetics [3], efflux rate and internalization of the liposomes by cells [4] and induction of immune responses in liposomal vaccines [5]. Lamellarity also seems to play an important role in model protocell membranes growth and division [6, 7] and in cells transfection [8].

Vesicular interfaces can be used as templates for protein adsorption either on bare [9, 10] or polysaccharide-modified [11] bilayers. Temperature-responsive polymers can be grafted onto liposomes in order to create nanocarriers where drug release is triggered at a tunable temperature [12, 13]. Additionally, pH-sensitive polyelectrolytes or hydrogel-liposome nanocomposites have shown potential for controlled release of bioactive substances [14, 15]. Hydrophobic mismatch controls the final shape in mixed polymer/phospholipid vesicles [16], defines the domain size in mixed phospholipids combined with cholesterol [17] and can be used in molecular rulers by the aid of amphiphatic peptides [18]. Amphiphilic copolymers based on poly(2-oxazoline) have proven potential for drug delivery applications [19]. They have been used as biomaterials in fibrous scaffolds [20], bioconjugates [21] and non-viral vectors [22]. In previous studies of our group, DPPC- MPOx chimeric liposomes have been

investigated. Their thermoresponsive character has been revealed by light scattering while loading and release properties were found to be dependent on the molar ratio of MPOx [23, 24].

There are several methods to prepare liposomes and it is very important to experimentally determine if the desired vesicular size and lamellarity are achieved [25]. SANS is a powerful method to probe length scales from 1 to 100 nm [26], and therefore to characterize the size distribution, lamellarity and bilayer structure in liposomal formulations [4] and to probe the lateral heterogeneities in vesicular membranes [16]. Small angle neutron and X-ray scattering have successfully resolved the structure, stimuli responsiveness and transformation kinetics in pharmaceutical liposomes [27] and detailed analytical methodologies have been applied to polymer-decorated liposomes [28]. Recently the effects of several factors as formulation method and phospholipid composition on liposome lamellarity were investigated with SANS showing that polymer-modified lipids may lead to uni-lamellar vesicle populations [4]. In this paper SANS experiments on DPPC liposomes and on DPPC liposomes with MPOx amphiphilic pseudodiblock copolymers are reported. Our analysis uses one single model to fit all the SANS data sets at all concentrations, temperatures and copolymer compositions. This model is a superposition of form factors from distinct populations of vesicles with different lamellarity and radius. The effect of temperature on the DPPC vesicles in the presence of MPOx and on the MPOx composition is resolved. The lamellarity and size changes that are observed as a function of temperature and hydrophobic content may be used to tune the thermal response of DPPC hybrid vesicles for drug and gene delivery applications.

2. Materials and methods

2.1 Materials

The phospholipid used for liposomal formulations was 1,2-dipalmitoyl-sn-glycero-3-phosphocholine (DPPC). It was purchased from Avanti Polar Lipids Inc. (Alabaster, AL, USA) and used without further purification. Chloroform and all other reagents were of analytical grade and purchased from Sigma-Aldrich Chemical Co. The gradient pseudodiblock copolymers poly(2-methyl-2-oxazoline)-grad-poly(2-phenyl-2-oxazoline) (MPOx) (Scheme 1) were prepared via cationic polymerization as described extensively elsewhere [29]. Deuterium oxide (D_2O) 99.90% was purchased from Euriso-top.

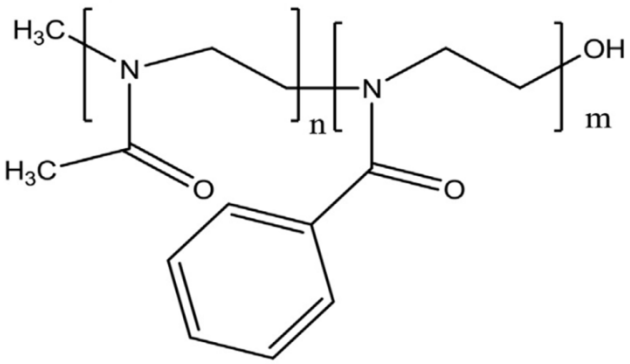

Scheme 1. Chemical structure of MPOx copolymers.

Two gradient MPOx copolymers were used in this study labeled as MPOx1 and MPOx2 corresponding to $MeOx_{51}$-grad-$PhOx_{10}$ and $MeOx_{28}$-grad-$PhOx_{9}$ respectively (where the subscripts denote number of monomers). MPOx1 and MPOx2 have molar mass 5200 and 3300 $gmol^{-1}$, polydispersity (M_w/M_n) 1.14 and 1.26 and hydrophobic content (PhOx) 28 and 39 %wt respectively. The copolymers were added by a molar ratio 10% in the total added molecules (DPPC and MPOx) which is 44% for MPOx1 and 33% for MPOx2 in mass percentage. In this composition the mass ratio of the hydrophobic

monomers (PhOx) were similar i.e. 18% for DPPC-MPOx1 and 16% for DPPC-MPOx2 mixtures.

2.2 Sample preparation

The systems were prepared by thin film hydration method as described in our previous studies [23, 24]. Briefly, the desired amounts of DPPC and MPOx were dissolved in chloroform/methanol (9:1 v/v) and mixed in a round flask. The mixed thin film was formed by slow removal of the solvent at 50 °C while the round flask was connected to a rotary evaporator (Rotavapor R-114, Buchi, Switzerland) with applied vacuum 1.0×10^{-2}mbar. The mixed phospholipid film was maintained under vacuum for at least 24 h in a desiccator to remove traces of solvent and afterwards hydrated in D_2O by slow stirring for 1 h in a water bath above the phase transition of lipids. The resultant aqueous solutions were subjected to two, 3 min and 3 min sonication cycles (amplitude 70, cycle 0.7) interrupted by a 3 min resting period, in water bath, using a probe sonicator (UP 200S, Dr. Hielsher GmbH, Berlin, Germany). The samples were allowed to anneal for 30 min.

The targeted concentration of DPPC in the final solutions of DPPC and DPPC-MPOx vesicles was 30 $mgml^{-1}$. Samples at nominal concentrations lower than 30 $mgml^{-1}$ were prepared by diluting the stock solutions by the proper amount of water solvent. The sample temperature was controlled by a Julabo thermostat with an accuracy of 0.01 °C and the samples were allowed to equilibrate for longer than 30 min at the desired temperature. The temperatures in the study (25, 37 and 45 °C) were chosen so that there was one temperature below (25 °C) and one above (45 °C) the transition of DPPC vesicles at 41-42 °C. The temperature 37 °C was chosen as it is the physiologically relevant temperature.

2.3 Small angle neutron scattering experiments

KWS-2 high intensity / wide-q SANS diffractometer (FRMII reactor at Jülich Centre for Neutron Science) was used for the experiments. Neutron wavelength λ=4.5 Å was used and the SANS wave vector (q) covered more than 2 orders of magnitude from 0.0014 to 0.51 $Å^{-1}$ combining three separate detection configurations (2, 8 and 20 m detection length). Raw data was treated by standard correction and reduction procedures. The collected 2-D raw data were found isotropic and were azimuthally integrated into 1-D scattered intensity $I(q)$. The q-independent incoherent scattering that appears as a flat background in SANS profiles was subtracted from the experimental data. Theoretical SANS profiles $I^{th}(q)$ were convoluted [30] with a Gaussian function in order to take instrumental resolution function $\Delta q(q)$ into account [31, 32] i.e. $I^{conv}(q) = \frac{1}{\sqrt{2\pi}\Delta q(q)} \int_{-\infty}^{+\infty} dq' \cdot exp\left(-\left(\frac{q'-q}{\sqrt{2}\Delta q(q)}\right)^2\right) \cdot I^{th}(q')$. Polydispersity was taken into account using a Gaussian distribution [33] of the vesicular internal radii (Discussion section) as $I^{poly}(q;R) = \frac{1}{\sqrt{2\pi}\Delta R} \int_0^{+\infty} dR' \cdot exp\left(-\left(\frac{R'-R}{\sqrt{2}\Delta R}\right)^2 \cdot I^{conv}(q;R')\right)$ where R is one of the radii. Fitting procedure included the calculation of $I^{poly}(q)$ and minimization of the sum of the weighted square differences $\chi^2 = \sum_{i=1}^{N}\left(\frac{I^{poly}(q_i)-I^{exp}(q_i)}{\delta I^{exp}(q_i)}\right)^2$ between N theoretical and experimental intensities, where $I^{exp}(q_i)$ is the experimentally obtained intensity and $\delta I^{exp}(q_i)$ its uncertainty. The calculations were made with custom made code in MATLAB. Fitting algorithms were based on a Monte Carlo simulated annealing minimization scheme [34].

3. Results and discussion

3.1 SANS on pure DPPC vesicles and justification of the fitting model

SANS measurements were performed in order to resolve the morphology of the solutions at length scales 1-100 nm. In Fig. 1a the SANS profiles from pure DPPC solutions at 25 ºC are shown. Intensity scales proportionally to concentration while their shape remains unchanged showing a concentration-independent form factor at this concentration range. Normalizing SANS intensity by concentration proves that the separate SANS profiles collapse on each other (Fig. S1 a1). The presence of vesicles is evident in the q-dependence of the scattered intensities at intermediate q (Fig. 1a). Neglecting mild modulations, a power-law $I(q)\sim q^{-2.6}$ is followed at intermediate q up to 0.1 Å^{-1}. This is reminiscent to scattering from planar interfaces [35] where $I(q)\sim q^{-2}$. A characteristic shoulder right next to the Guinier regime (0.01-0.013 Å^{-1} in Fig. 1) is what normally appears for thin hollow spherical or ellipsoidal vesicles and is determined by the overall vesicular size [35-37]. At q > 0.1 Å^{-1} the strong drop in $I(q)$ and the shoulder at q ≈ 0.2 Å^{-1} is related to the thickness and density profile of the bilayers [38].

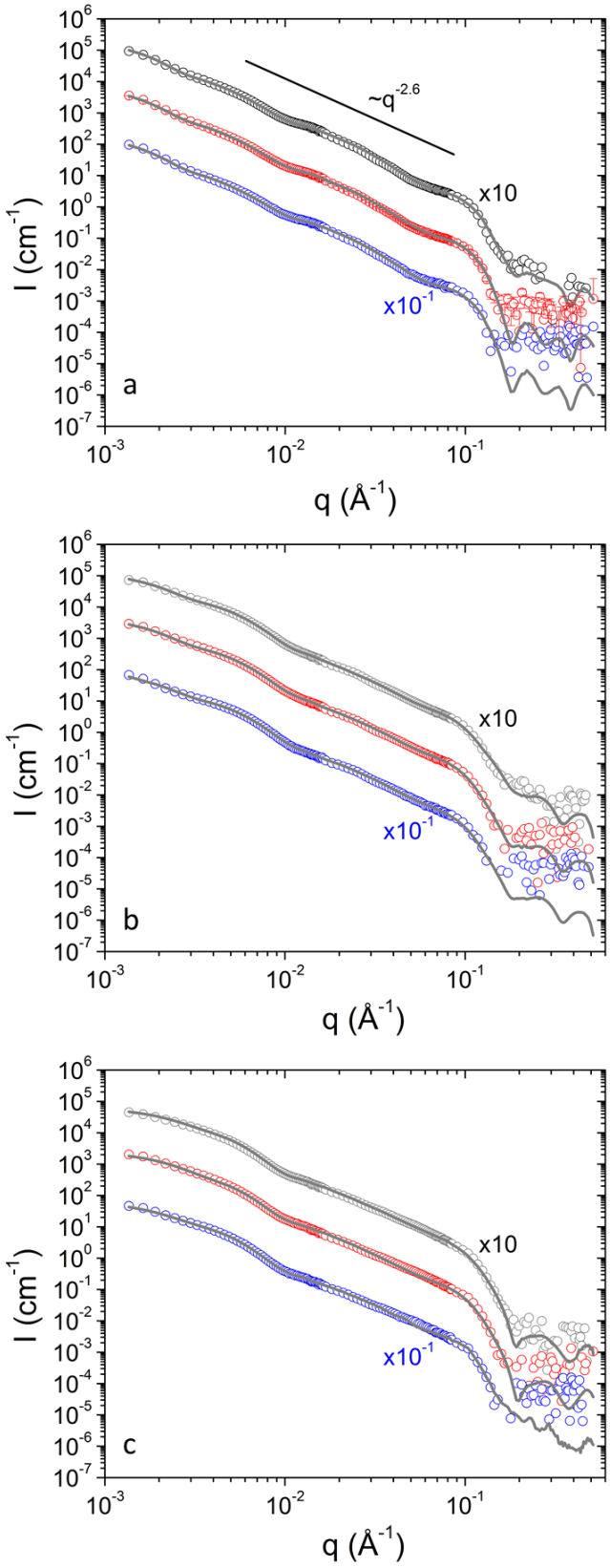

Fig 1. SANS from 3 (blue), 10 (red) and 30 (gray) mgml^{-1} DPPC in D_2O at (a) 25 °C, (b) 37 °C and (c) 45 °C. Error bars are included for 10 mgml^{-1} in (a). Lines are fits to

the experimental data. Straight line indicates power-law behavior. Profiles are shifted vertically for clarity as shown.

The form factors of spherical vesicles were employed to fit the experimental curves as it was dictated by the SANS profiles. The model that was used will be analyzed in the following, however, at this point a qualitative description of its choice will be made. The scaling $I(q)\sim q^{-2.6}$ at intermediate length scales is not possible to fit with vesicles of a single population even by the introduction of polydispersity. In Fig. S2 it is proved that the use of a single population of uni-lamellar vesicles does not follow the data at low and intermediate q neither the shoulder at 0.1 Å^{-1}. The superposition of another population of bi-lamellar vesicles with larger size is necessary to create an apparent scaling that is stronger than $I(q)\sim q^{-2}$. The best fit was provided by the superposition of polydisperse small-size uni-lamellar and large-size bi-lamellar vesicles. This model could follow both the intermediate q scaling and the modulations on the scattering curves (Fig.1 and S 2). Illustrative examples of such modulations are the deep at 0.06 Å^{-1} and the shoulder at 0.1 Å^{-1}. The strong oscillation introduced by the bi-lamellar interface creates the aforementioned features especially the shoulder at 0.1 Å^{-1} which cannot be reproduced by uni-lamellar vesicles independently on their radius. On the other hand, combination of two bi-lamellar vesicle populations creates strong deeps at about 0.06 and 0.18 Å^{-1} that do not appear in the experimental data. It has to be kept in mind that the scattering at high q is mostly defined by the bilayer structure and its lamellarity and not by the overall radius. The need of the superposition of two sizes of vesicles is also evident at low q. The small-size vesicles reproduce the deep at 0.01 Å^{-1}. However scattering increases strongly towards lower q values while at this region small-size vesicles contribute by a Guinier "plateau". The contribution of large-size vesicles

greatly enhances scattering at low q (Fig. S2). Combination of uni- and bi-lamellar layers observed by SANS has been also reported by Nele et al. on DPPC vesicles prepared by thin film hydration methods [4]. Finally, a correction is provided by the terms $S_1(q)$ and $S_2(q)$ for uni- and bi-lamellar vesicles respectively to fully reproduce the experimental data as described in the following. Polydispersities were introduced as fitting parameters. The values $\Delta R/R$~30% for small-size vesicles (10-20 nm) and ~40% for large-size vesicles (80-100 nm) were the optimal values for all fits. These ranges of polydispersities are common in liposomal systems [39, 40].

The experimental data from DPPC vesicles (including mixtures with MPOx copolymers) were fitted with a model that is based on uni-lamellar and multi-lamellar polydisperse spherical vesicles (equation 1). Herein multi-lamellar vesicles refer to vesicles with lamellarity that is greater than 1. In spherical symmetry the scattering amplitude [35, 41, 42] is $A(q) = \int_0^\infty 4\pi r^2 \frac{sinqr}{qr} \Delta\rho(r) dr$. Where $\Delta\rho(r)$ is the average radial profile of the neutron scattering length density (SLD) contrast between the particle and the solvent. The scattered intensity of equation 1 corresponds to scattering from N separate populations of vesicles.

$$I(q) = \sum_{i=1}^{N} N_i \cdot |A_i(q)|^2 \cdot S_i(q) \qquad (1)$$

Where N_i is the number concentration of uni-lamellar ($i = 1$), bi-lamellar ($i = 2$) etc vesicles. The scattering amplitude $A_i(q)$ of a single vesicle consisting of i layers is defined in equation 2.

$$A_i(q) = \sum_{j=1}^{i} A_{bilayer}(q, B_{out}, B_{in}, R_i, d_{out}, d_{in}) \qquad (2)$$

Where R_i is the internal radius of the vesicle, d_{out} the thickness of the two external layers and d_{in} the thickness of the inner layer of the bilayer. The scattering amplitude of a single bilayer is the superposition of the scattering amplitudes of three separate shells (lamellae).

$$A_{bilayer}(q, B_a, B_b, R, d_a, d_b) = A_{shell}(q, B_a, R, R + d_a) + A_{shell}(q, B_b, R + d_a, R + d_a + d_b) + A_{shell}(q, B_a, R + d_a + d_b, R + d_a + d_b + d_a) \quad (3)$$

with

$$A_{shell}(q, B, R, R') = \frac{4\pi B}{q^3} \cdot \left((sinqR' - qR'cosqR') - (sinqR - qRcosqR)\right) \quad (4)$$

The contrast factors B are defined in equations 5a and b.

$$B_{out} = \rho_h - \rho_w \quad (5a)$$

$$B_{in} = \rho_t - \rho_w \quad (5b)$$

Where ρ_w is the neutron SLD of the water solvent and it is the volume average of the scattering length densities of D_2O ($\rho_{D2O} = 6.4 \cdot 10^{-6}\text{Å}^{-2}$) and H_2O ($\rho_{H2O} = -0.56 \cdot 10^{-6}\text{Å}^{-2}$). The SLDs of the head and tail layers are ρ_h and ρ_t and denote the hydrophilic and hydrophobic part of the bilayer respectively. An illustration of the vesicular structure and the lamellar formations in uni- and bi-lamellar vesicles is shown in scheme 2.

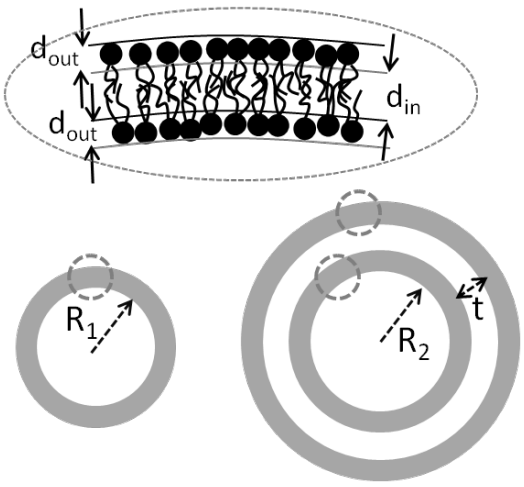

Scheme 2. Illustration of uni-lamellar and bi-lamellar DPPC vesicles. Regions within dashed circles are enlarged in order to demonstrate the fine structure of the membrane interfaces. Hydrophilic heads and hydrophobic tails of the phospholipids are presented by black circles and curly lines respectively.

The factors $S_i(q)$ in equation 1 are introduced by Debye terms and are provided by equation 6 as they were proved to be necessary for the fitting at low q. They correspond to dimmers of vesicles with centre-to-centre distance D_i [42, 43]. The prefactor n_i equals 1 when all vesicles are in pairs and 0 when they are all in unimeric state (i.e. $S_i(q) = 1$). Hence n_i represents the ratio of the number of vesicles that take part in pairs over the total number of vesicles. Values of n higher than 1 indicate presence of aggregates containing more than 2 vesicles.

$$S_i(q, n_i, D_i) = 1 + n_i \cdot \frac{sinqD_i}{qD_i} \qquad (6)$$

SANS parameters can be used to calculate the number and mass ratios of different vesicle populations. The details of the calculations are presented in Supplementary Material.

The optimal fitted values of the SLDs for the tail and head regions were $\rho_t = 2.70 \cdot 10^{-6}$ Å^{-2} and $\rho_h = -0.31 \cdot 10^{-6}$ Å^{-2} respectively and are compatible with other works either on DPPC vesicles in solution [38] or DPPC membranes on the solid water interface [44, 45]. These values provided good fits for all data sets in this study for lamellarities and all temperatures and concentrations in DPPC, DPPC-MPOx1 and DPPC-MPOx2 liposomes. The hydrocarbon region in DPPC consists of the lipid tails (Scheme S1) and it is normally reported to have a size of about 2.8-3.5 nm at room temperature [38, 40, 44, 46]. In our case the resulting thickness of the tail region is $d_{in} = 2.92$ nm (Table 1). The size of the head groups region is reported at 0.9-1.1 nm while in our case is $d_{out} = 0.64$ nm. This discrepancy of about 0.26 nm could be related to the fact that our fitting model does not include any interdigitation of the separate layers that normally are taken into account by gradually varying profiles as a function of radial distance.

Table 1. SANS parameters extracted for DPPC solutions at all temperatures (T) and concentrations (c). Contributions to the model from uni- and bi- lamellar vesicles are indicated as a and b respectively. Number ratios $N_a/(N_a+N_b)$, mass ratios $m_a/(m_a+m_b)$, thickness of the external and inner layers d_{out} and d_{in} respectively of the bilayers, internal radii of the vesicles $R_{a,b}$, thickness of the inter-bilayer spacing t, characteristic d-spacing of the multilayers and prefactors $n_{a,b}$ for the Debye terms are presented (uncertainties: in number and mass percentage ~0.5%, in radii and thicknesses ~7%, in prefactors n_i ~1%~~, in c_{SANS} ~0.5%~~).

T (°C)	25			37			45		
c (mgml^{-1})	3	10	30	3	10	30	3	10	30
model	a=uni and b=bi								
$N_a/(N_a+N_b)$	0.99	0.99	0.99	0.99	0.99	0.99	0.99	0.98	0.98
$m_a/(m_a+m_b)$	0.22	0.23	0.24	0.50	0.45	0.42	0.61	0.58	0.66
d_{out} (nm)	0.64	0.64	0.64	0.66	0.66	0.66	0.65	0.65	0.65
d_{in} (nm)	2.92	2.92	2.92	2.59	2.59	2.59	2.24	2.24	2.24
R_a (nm)	20.1	20.6	20.1	22.2	22.4	22.1	21.8	21.9	22.1
R_b (nm)	115	116	114	94.2	93.8	94.6	67.7	66.3	64.9
t (nm)	1.27	1.26	1.27	1.59	1.58	1.56	1.85	1.85	1.85
d-spacing (nm)	5.47	5.46	5.47	5.50	5.49	5.47	5.39	5.39	5.39
n_{1a}	2.16	2.22	2.16	2.11	2.09	2.29	1.59	1.71	1.89
n_{2b}	0.77	0.78	0.76	1.34	1.40	0.68	1.17	1.34	1.33
~~c_{SANS} (mgml^{-1})~~	~~2.01~~	~~7.32~~	~~23. 1~~	~~1.10~~	~~5.22~~	~~21.1~~	~~1.10~~	~~4.71~~	~~15.0~~

In Fig. S1 (b1 and c1) it is shown that the concentration dependence of the SANS profiles in DPPC is trivial i.e. the form factor is unaltered, also at 37 and 45 °C. This is also reflected on the extracted parameters of Table 1. The dependence of the SANS profiles of DPPC on temperature is shown in Fig. 2. At low q the scattered intensity shows a weak drop as a function of temperature indicating that the large size vesicles change in size and/or number. At the intermediate q range the curvature features of the profiles gradually diminish which shows that the relative contribution of uni-lamellar vesicles is enhanced. These observations are reflected in the fitted parameters of Table 1. All data sets from DPPC at all temperatures were modeled by the combination of uni- and bi-lamellar vesicles. The quality of the fits is demonstrated in Fig. 1a-c. The

size R_a (~21 nm) of the small size liposomes remains unchanged which has been also observed elsewhere for uni-lamellar DPPC vesicles [47]. The large vesicles size gradually decreases as their internal radius R_b drops from 115 to 65 nm. As the size of the large vesicles decreases their contribution becomes weaker and the scattering at low q drops. The number percentage of the small uni-lamellar vesicles is the same at all temperatures or slightly smaller at 45 °C (10 and 30 mgml^{-1}). However, their mass percentage rises gradually from about 23% at 25 °C to about 62% at 45 °C because the size of the large vesicles and consequently their mass drops. Decrease of the radius of DPPC liposomes as a function of temperature has been reported elsewhere and it was attributed to the decrease of the membrane rigidity upon the gel-to-liquid crystalline phase transition that allows bending of the interface to higher curvatures [Soft Matter, 2010,6, 1352-1360].

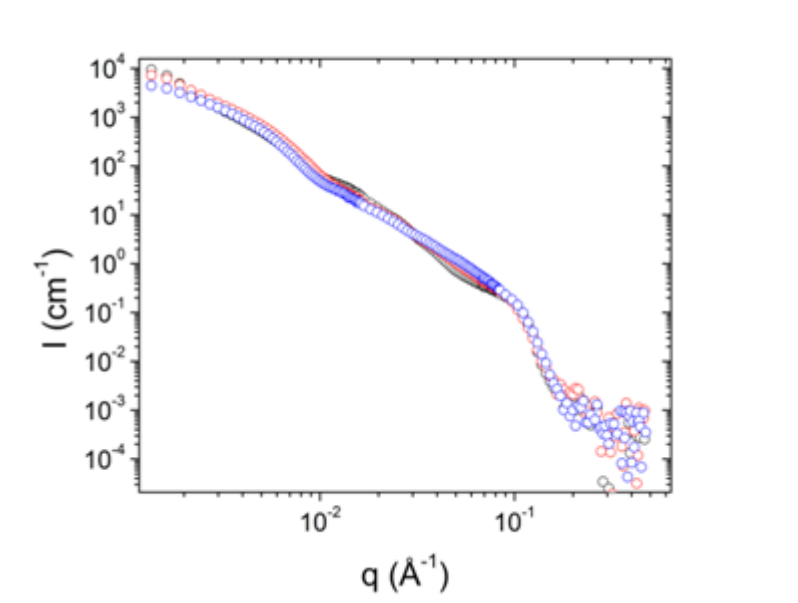

Fig 2. SANS from 30 mgml^{-1} DPPC in D_2O at 25 (black), 37 (red) and 45 (blue) °C.

DPPC liposomal membranes are expected to go through a temperature phase transition at 41-42 °C. This has been investigated experimentally [46], by coarse grained model

simulations [48] and with both experiments and simulation [44]. The lipid bilayer membrane changes from a gel phase to a liquid crystalline phase upon temperature increase. At the same time the hydrocarbon tail region shrinks while the head group thickness remains practically unchanged [44, 46, 47]. The change in the high q scattering is accompanied by a gradual shrinkage of the hydrophobic layer d_{in} from 2.92 to 2.24 nm while the size of the head group area d_{out} is unaltered in accordance to the aforementioned previous studies [44, 46, 47]. A gradual decrease of the bilayer thickness has been also reported by Gallová et al. [49] and covered the range 33-45 °C.

3.2 Concentration and temperature dependence in DPPC-MPOx1 vesicles

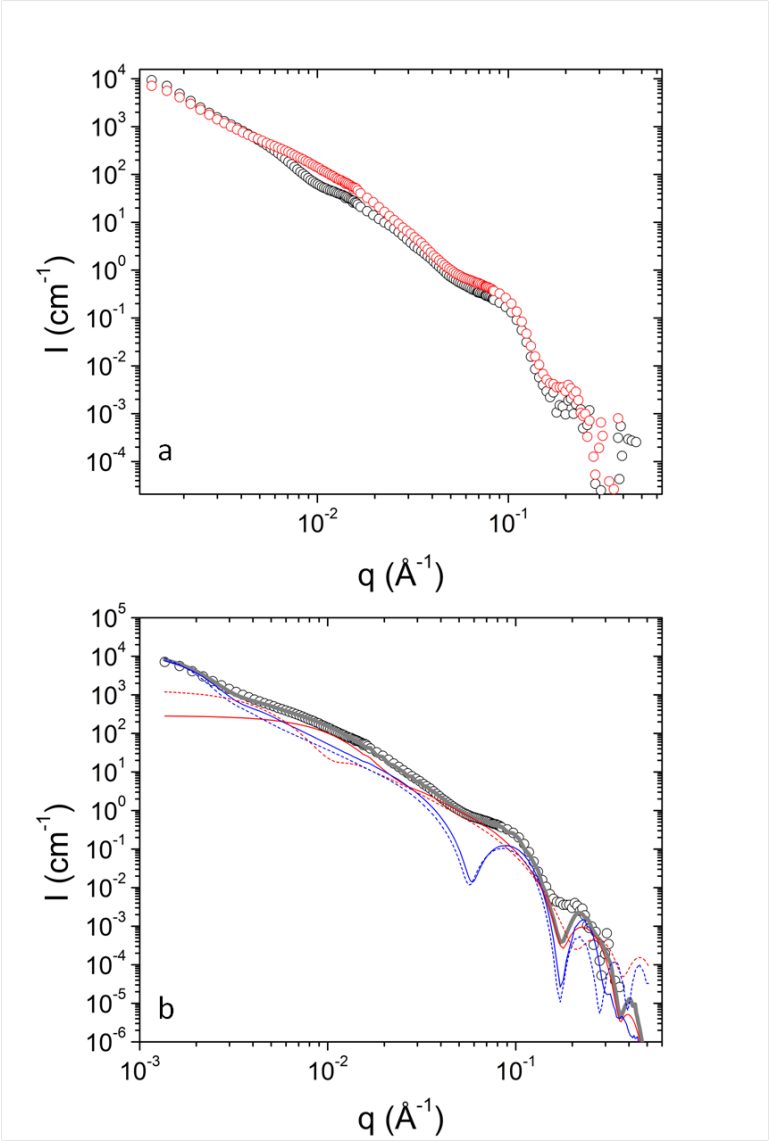

Fig 3. (a) SANS from DPPC (black) and DPPC-MPOx1 (red) at 30 mgml^{-1} in D_2O at 25 °C. (b) Contributions from uni-lamellar (small-size) vesicles (red) and bi-lamellar (large-size) vesicles (blue) on the fitting curve (gray) on SANS from 30 mgml^{-1} DPPC-MPOx1 in D_2O at 25 °C. Dotted lines correspond to contributions from fits from pure DPPC vesicles under the same conditions.

Scattering profiles from DPPC-MPOx1 at q > 0.02 Å^{-1} have similar shape as the ones from pure DPPC (Fig. 3a). This indicates that local bilayer structure (high q) is the same as in DPPC regarding SANS profiles. The thicknesses (d_{in} and d_{out}) of bilayers are

practically unchanged (Tables 1 and 2). However, any alterations in the bilayer that were at very small length scale would not be resolved as our SANS intensity is very weak at q > 0.2-0.3 $Å^{-1}$. The effect of incorporation of MPOx in the liposomal preparation causes measurable changes that relate to the number and the overall size of the vesicles (and in their mass concentration, Section 3.4). The inner radius (R_a) of small-size vesicles shrinks from 20 to 9 nm while their relative number density (N_a) increases. Similarly, for the large-size vesicles R_b decreases from 114 to 90 nm while their relative number density (N_b) decreases. These changes can be clearly visualized in Fig. 3b where the Guinier plateau regions (especially for uni-lamellae) shift to higher q in comparison to DPPC while at high q they coincide. It is clear, that this effect increases the scattered intensity at 0.01 $Å^{-1}$ (Fig. 3a) and compensates for the experimentally observed increase in the presence of MPOx1. The incorporation of MPOx1 creates formulations that are stable at smaller radii of curvature as observed previously [50]. In mixed surfactant uni-lamellar vesicles of the cationic cetyl trimethylammonium tosylate (CTAT) and the anionic sodium dodecyl benzene sulfonate (SDBS), addition of hydrophobically modified chitosan at low concentrations led to a 50% decrease in radius. The authors suggested that the addition of polymer increases the interfacial bending rigidity which results to higher curvatures [51].

Table 2. SANS parameters extracted for DPPC-MPOx1 solutions at all temperatures (T) and concentrations (c). Contributions to the model from uni- and bi- lamellar vesicles are indicated as a and b respectively. Number ratios $N_a/(N_a+N_b)$, mass ratios $m_a/(m_a+m_b)$, thickness of the external and inner layers d_{out} and d_{in} respectively of the bilayers, internal radii of the vesicles $R_{a,b}$, thickness of the inter-bilayer spacing t, characteristic d-spacing of the multilayers and prefactors $n_{a,b}$ for the Debye terms are

presented (uncertainties: in number and mass percentage ~0.5%, in radii and thicknesses ~7%, in prefactors n_i ~1%~~, in c_{SANS} ~ 0.5%~~).

T (°C)	25			37			45		
c ($mgml^{-1}$)	3	10	30	3	10	30	3	10	30
model	a=uni and b=bi			a=uni and b=uni			a=uni and b=uni*		
$N_a/(N_a+N_b)$	0.992	0.993	0.995	0.983	0.986	0.988	0.988	0.992	0.995
$m_a/(m_a+m_b)$	0.17	0.18	0.22	0.17	0.19	0.22	0.18	0.27	0.37
d_{out} (nm)	0.63	0.65	0.64	0.61	0.63	0.64	1.02	0.96	0.94
d_{in} (nm)	2.85	2.96	2.92	2.86	2.92	2.92	2.46	2.62	2.59
R_a (nm)	9.62	9.44	9.01	9.22	9.03	9.03	9.45	9.94	9.95
R_b (nm)	89.5	89.3	88.8	91.2	86.3	89.2	103	105	102
t (nm)	1.75	1.75	1.25	-	-	-	-	-	-
d-spacing (nm)	5.86	6.01	5.45	-	-	-	-	-	-
n_a	1.19	1.28	1.26	1.47	1.67	1.58	2.97	2.15	1.9
n_b	0.42	0.39	0.35	1.27	0.96	0.77	-	-	-
~~c_{SANS} ($mgml^{-1}$)~~	~~2.51~~	~~8.02~~	~~22.1~~	~~2.50~~	~~7.92~~	~~22.1~~	~~3.31~~	~~11.0~~	~~27.1~~

*No Debye term was used i.e. $S_i(q) = 1$.

The temperature response of DPPC-MPOx1 is shown in Fig. 4. The concentration dependence in DPPC-MPOx1 is trivial (Fig. S1 a2, b2 and c2) and therefore comparison of SANS profiles of different temperatures at 30 $mgml^{-1}$ is representative for all concentrations. The SANS profiles at 37 and 45 °C have a weaker drop in the region 0.02-0.09 $Å^{-1}$ and lack of the characteristic shoulder at 0.1 $Å^{-1}$ in comparison to 25 °C (Fig. 4). The temperature response of the MPOx1-containing liposomes is qualitatively different than the one of the pure DPPC liposomes. In liposomes of pure DPPC, changes in temperature did not affect lamellarity. The effects were on the hydrophobic tail region and on the size of the large vesicles. However, in DPPC-MPOx1 at 37 and 45°C the model changes from a combination of uni- and bi-lamellar to a combination of two uni-lamellar vesicles (Table 2). At 45 °C the large vesicles are in the unimeric state as $S_2(q) = 1$.

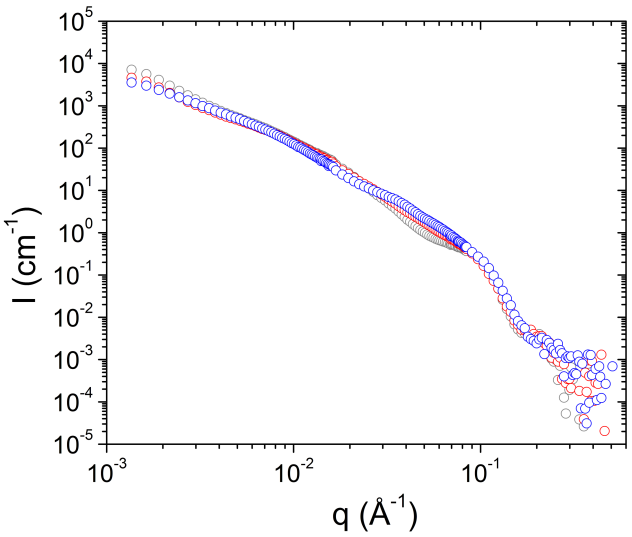

Fig 4. SANS from DPPC-MPOx1 30 mgml^{-1} in D_2O at 25 °C (gray), 37 °C (red) and (c) 45 °C (blue).

The internal radius (R_a) of the original uni-lamellar vesicles remains unchanged from 25 to 45 °C. The original bi-lamellar vesicles transform into uni-lamellar vesicles with similar internal radius (R_b) at 90 nm while the bilayer parameters (d_{in} and d_{out}) remain the same. From 37 to 45 °C d_{in} decreases from 2.9 nm to 2.6 nm as it was the case in DPPC due to the gel-to-liquid crystalline phase transition (Table 2). However, the thickness of the hydrated layer d_{out} increases from 0.64 nm to 0.97 nm which points to presence of MPOx chains on the water/bilayer interface. The mostly hydrophilic end of the gradient copolymer is expected to have the tendency to contact the aqueous environment (in the following a detailed discussion on the incorporation of MPOx in the vesicles based on their mass concentration will be made, Section 3.4). At the same time there is an increase in the internal radius (R_b) of the large vesicles. The mass percentage of different vesicles are similar to the ones of pure DPPC at 25 ºC but remain practically unchanged as temperature increases. The quality of the fits at all concentrations and temperatures for DPPC-MPOx1 are shown in Fig. 5.

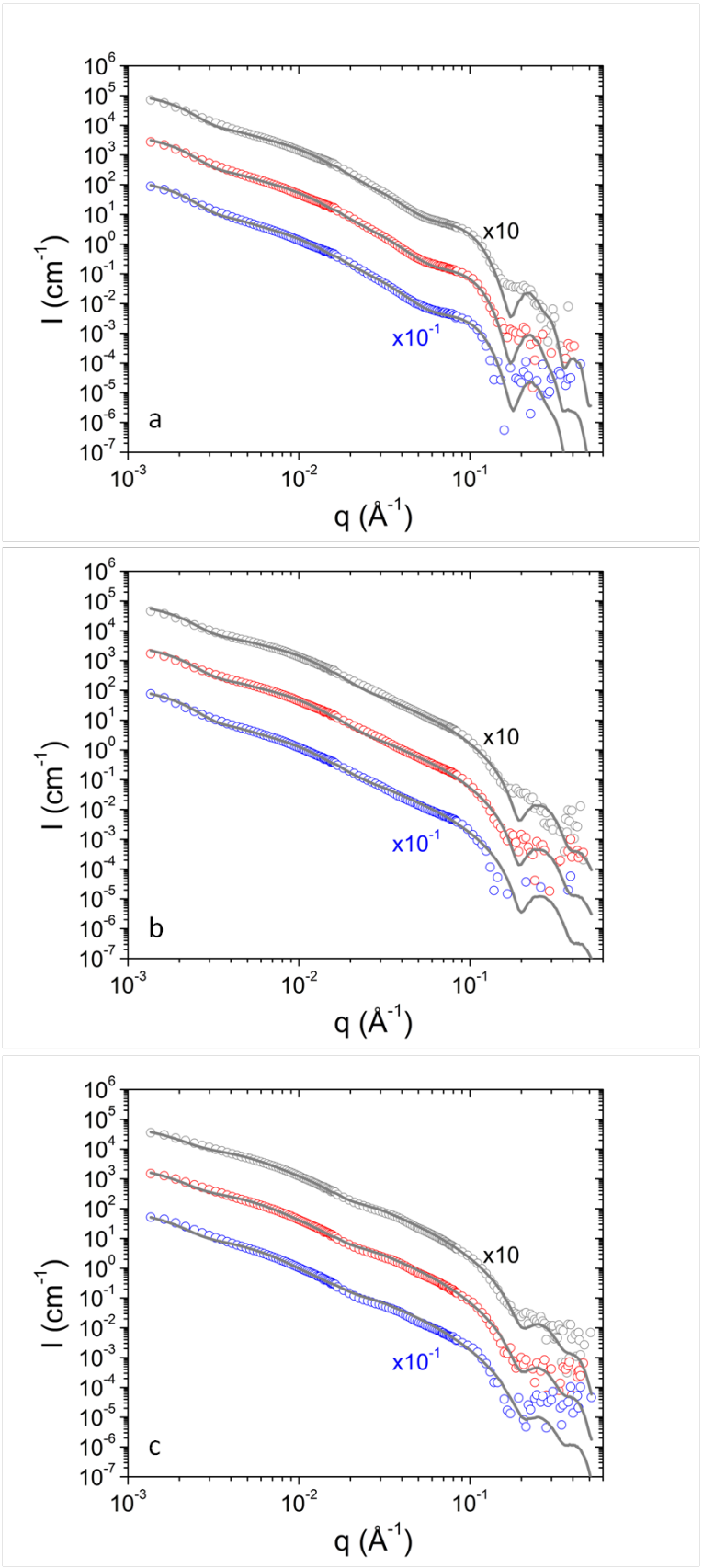
I (cm^{-1})
q (Å^{-1})
x10
x10^{-1}
a
b
c

Fig 5. SANS from 3 (blue), 10 (red) and 30 (gray) mgml^{-1} DPPC-MPOx1 in D_2O at (a) 25 °C, (b) 37 °C and (c) 45 °C. Lines are fits to the experimental data. Profiles are shifted vertic7ally for clarity as shown.

It is well-accepted that stabilization of uni-lamellar vesicles against the formation of vesicles of higher lamellarity is achieved by two different mechanisms. At values of bending constant in the order of k_BT Helfrich undulations result to a repulsive interbilayer potential. At higher bending constants spontaneous curvature stabilizes the vesicles at an energetically preferable radius excluding multiple bilayers [https://doi.org/10.1073/pnas.98.4.1353]. In the case of DPPC-MPOx1 vesicles the increased presence of MPOx chains is evident especially at 45 °C by the increase in the thickness of the outer layer and the mass of the vesicles (section 3.4). Their hydrophilic segments in the interbilayer spacings enhance the repulsive interbilayer potential and destabilize bi-lamellar vesicles at temperatures above 25 °C. It has to be noted that the gel-to-liquid crystalline phase transition that leads to a reduction of the bilayer stiffness may also assist the destabilization of bi-lamellar vesicles.

3.3 Concentration and temperature dependence in DPPC-MPOx2 vesicles

The SANS data from DPPC-MPOx2 (Fig. 6a) at 25 °C is completely different from the corresponding data from DPPC and the ones from DPPC-MPOx1. MPOx2 causes dramatic changes in the scattering profiles. This relates to its higher relative hydrophobic content as it has a smaller number of hydrophilic monomers than MPOx1. This possibly allows MPOx2 to interact more strongly with the hydrophobic interior of the DPPC bilayers. Two characteristic peaks appear at high q i.e. $q_1^* \approx 0.105$ Å^{-1} and $q_2^* \approx 2q_1^* \approx 0.211$ Å^{-1}. These peaks correspond to multi-lamellar formulations in the

solution. Using Bragg's law they correspond to a characteristic d-spacing $d = \frac{2\pi}{q_1^*} \approx 6\ nm$ which is compatible with other works on DPPC multilamellar vesicles [4]. This value agrees with the total thickness of a single lamellar layer including a water layer between successive bilayers. This is $d = d_{in} + 2d_{out} + t$ and it is about 5-6 nm (tables 1, 2 and 3). The scattering at q < 0.01 Å^{-1} is significantly enhanced showing a stronger q dependence in comparison to DPPC and relates to vesicles of large mass as will be discussed in the following.

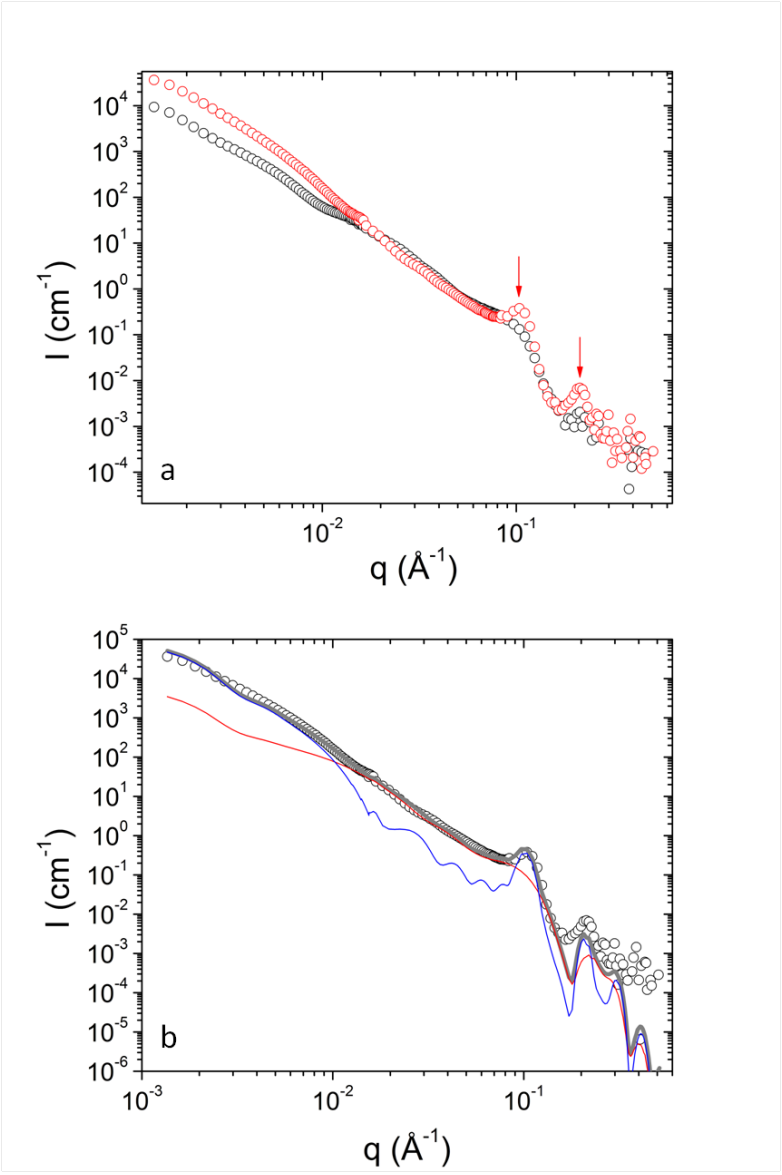

Fig 6. (a) SANS from DPPC (black) and DPPC-MPOx2 (red) at 30 mgml^{-1} in D_2O at 25 °C. Arrows indicate characteristic peaks. (b) Combined contributions from uni-lamellar and bi-lamellar vesicles (red) and contribution from hexa-lamellar vesicles (blue) to the fitting curve (gray) on SANS from 30 mgml^{-1} DPPC-MPOx2 in D_2O at 25 °C.

In Fig. 6b the fitting of the theoretical model to the SANS data from DPPC-MPOx2 at 25 °C is illustrated. The original model of DPPC vesicles (uni- and bi-lamellar vesicles) is superimposed with a multi-lamellar vesicles model in order to fit the low q scattering and the two peaks at high q. The best fit was achieved by superimposing a hexa-lamellar vesicle model. It is interesting that the internal characteristics of the membranes (d_{out} and d_{in}) remain similar to the ones of fits on DPPC and DPPC-MPOx1 (Table 3). Hence the presence of MPOx2 drives the creation of higher order lamellar structures. The mass percentage of hexa-lamellar vesicles is significant (75-85%). The size of uni- and bi-lamellar vesicles are similar to the ones in DPPC-MPOx1. The internal radius of the hexa-lamellar vesicles is about 80 nm (Table 3). In DPPC-MPOx2 the presence of the polymer with higher hydrophobic content stabilizes multi-lamellar vesicles of higher lamellarity in comparison to DPPC-MPOx1 because of the enhancement of attractive hydrophobic interactions between the separate bilayers and the high amount of added polymer (section 3.4). A similar effect was reported for the transition from uni- to bi-lamellar vesicles in the case of the addition of hydrophobically modified chitosan mentioned in the previous section [51].

Table 3. SANS parameters extracted for DPPC-MPOx2 solutions at all temperatures (T) and concentrations (c). Contributions to the model from uni-, bi-, tri- and hexa-lamellar vesicles are indicated. Number ratios $N_{a,b}/(N_a+N_b+N_c)$, mass ratios $m_{a,b}/(m_a+m_b+m_c)$, thickness of the external and inner layers d_{out} and d_{in} of the bilayers respectively, internal radii of the vesicles $R_{a,b,c}$, thickness of the inter-bilayer spacing t, characteristic d-spacing of the multilayers and prefactors $n_{a,b,c}$ for the Debye terms are presented (uncertainties: in number and mass percentage ~0.5%, in radii and thicknesses 7%, in prefactors n_i ~1%~~, in c_{SANS} ~0.5%~~).

T (°C)	25			37			45		
c (mgml^{-1})	3	10	30	3	10	30	3	10	30
Model	a=uni, b=bi and c=hexa			a=uni and b=uni	a=uni* and b=uni*		a=uni* and b=tri*		a=uni* and b=uni*
$N_a/(N_a+N_b+N_c)$	0.992	0.993	0.992	0.819	0.930	0.961	0.983	0.991	0.962
$N_b/(N_a+N_b+N_c)$	0.003	0.004	0.004	-	-	-	-	-	-
$m_a/(m_a+m_b+m_c)$	0.038	0.050	0.048	0.047	0.13	0.21	0.46	0.30	0.26
$m_b/(m_a+m_b+m_c)$	0.13	0.26	0.26	-	-	-	-	-	-
d_{out} (nm)	0.68	0.67	0.68	0.62	0.62	0.63	0.72	0.60	0.61
d_{in} (nm)	2.80	2.83	2.81	3.11	3.10	3.00	2.94	3.07	3.00
R_a (nm)	7.02	6.97	6.97	16.5	16.5	16.0	25.9	17.00	16.60
R_b (nm)	93.6	93.6	93.7	93.5	93.5	91.5	71.9	86.6	86.2
R_c (nm)	82.9	82.8	82.5	-	-	-	-	-	-
t (nm)	1.97	1.94	1.95	-	-	-	1.93	2.09	2.39
d-spacing (nm)	6.13	6.11	6.12	-	-	-	6.31	6.36	6.61
n_a	2.28	2.91	2.58	1.67	-	-	-	-	-
n_b	0.67	0.83	0.74	0.76	-	-	-	-	-
n_c	0.82	0.78	0.81	-	-	-	-	-	-
~~c_{SANS} (mgml^{-1})~~	~~4.21~~	~~14.0~~	~~40.1~~	~~4.31~~	~~17.1~~	~~48.1~~	~~1.81~~	~~12.0~~	~~38.1~~

*No Debye term was used i.e. $S_i(q) = 1$.

The decrease of the radii of uni- and bi-lamellar vesicles by incorporation of MPOx1 is also found for MPOx2 (Tables 1, 2 and 3). In the aforementioned CTAT/SDBS vesicular system, addition of hydrophobically modified chitosan at mass concentrations comparable to the surfactant mixture concentration resulted to the appearance of bi-lamellar and multi-lamellar vesicles [51] as it was observed by SANS. It has to be

mentioned that the multi-lamellar vesicles were of size that exceeded the q-window of SANS. Earlier studies had shown that the strength of the interaction with hydrophobically modified polyelectrolytes (at high salt conditions) and the resulting increase in vesicle rigidity increased as a function of hydrophobic content. In any case, the conformational-entropy loss during polymer adsorption is counter-balanced by the free energy of hydrophobic attraction [52].

The temperature response of DPPC-MPOx2 is presented in Fig. 7 separately for every concentration as concentration dependence is non-trivial at 45 °C (Fig. S1 a3, b3 and c3). At 30 mgml^{-1} above 25 °C the form factor does not contain the characteristic peaks. At lower concentrations a signature of peaks seems to re-appear at 45 °C. The quality of the fits at all concentrations and temperatures for DPPC-MPOx2 are shown in Fig. 8.

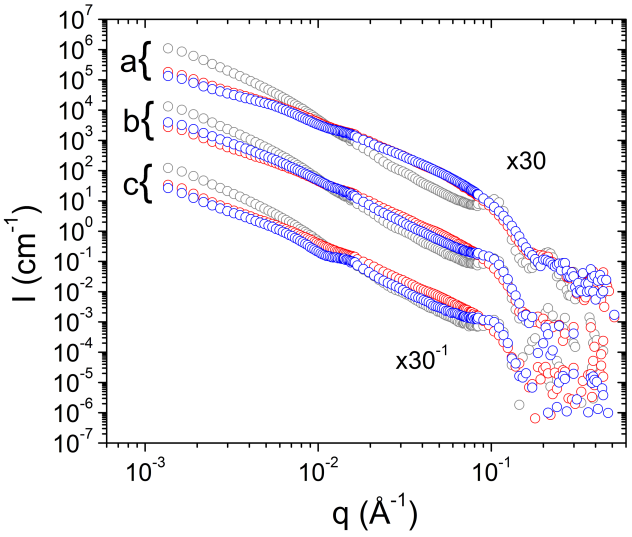

Fig 7. SANS from DPPC-MPOx2 at (a) 30 mgml^{-1}, (b) 10 mgml^{-1} and (c) 3 mgml^{-1}, in D_2O at 25 °C (gray), 37 °C (red) and (c) 45 °C (blue). Profiles are shifted vertically for clarity as shown.

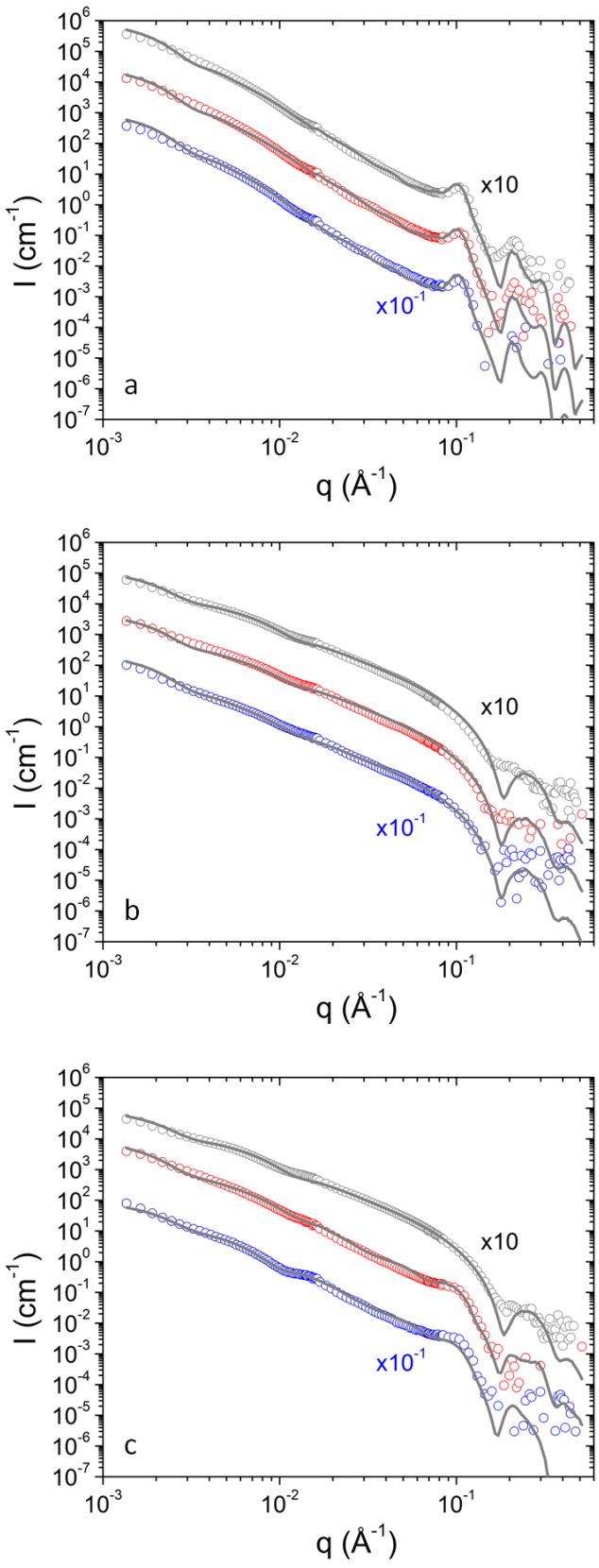
I (cm^{-1})
q (Å^{-1})
x10
x10^{-1}
a
b
c

Fig 8. SANS from 3 (blue), 10 (red) and 30 (gray) mgml^{-1} DPPC-MPOx2 in D_2O at (a) 25 °C, (b) 37 °C and (c) 45 °C. Lines are fits to the experimental data. Profiles are shifted vertically for clarity as shown.

The temperature response of the DPPC-MPOx2 liposomes from 25 to 37 °C leads to a combination of uni-lamellar vesicles similar to DPPC-MPOx1 liposomes. The multi-lamellar structures (bi- and hexa-) dissolve in uni-lamellar structures in favor of large uni-lamellar vesicles (Table 3). However, this is not the case for 45 °C (Fig. 7 and 8). Surprisingly multi-lamellar vesicles appear again in a manner that is concentration dependent. It is noted that no significant concentration dependence has been observed in terms of temperature response of lamellarity for DPPC and DPPC-MPOx1. At 30 mgml^{-1} only uni-lamellar vesicles are present (Table 3). Transformation of the large uni-lamellar vesicles to tri-lamellar vesicles is found at 10 mgml^{-1} with 70% in mass percentage and at 3 mgml^{-1} with 54% in mass percentage. At 37 °C for 10 and 30 mgml^{-1} and at 45 °C for all concentrations all vesicles are in the unimeric state and $S_i(q) = 1$. In the case of DPPC-MPOx2 a complex balance between interbilayer hydrophobic attraction (PhOx segments), interbilayer excluded volume repulsion (MeOx segments) and intrinsic membrane fluctuations (above the gel-to-liquid crystal transition) whose separate contributions depend on the amount and conformation of the copolymer on the bilayers lead to this peculiar temperature response of lamellarity.

In conclusion, as temperature increases the number of lipids in uni-lamellar versus bi-lamellar vesicles is enhanced in DPPC, bi-lamellar vesicles completely dissolve into uni-lamellar vesicles in DPPC-MPOx1 and multi-lamellar vesicles (bi- and hexa-) transform into uni-lamellar vesicles (except from the appearance of tri-lamellar vesicles at 3 and 10 mgml^{-1} at 45 °C) in DPPC-MPOx2. Therefore, there is a general trend of

the multi-lamellar vesicles to transform into uni-lamellar vesicles in a thermoresponsive manner which is more effective in the presence of MPOx copolymers.

3.4 Evaluation of vesicular concentration in pure DPPC and mixed DPPC-MPOx

Except from the changes on the lamellarity and size of the separate vesicular entities that prove the interaction between MPOx and DPPC liposomes one can estimate the mass concentration c_{SANS} in equivalent mass concentration of lipids (Supplementary Material). In the case of mixed DPPC-MPOx systems any excess mass concentration in comparison to pure DPPC solutions can be related to the presence of MPOx. Although the experiment's resolution at high q does not allow for a detailed description of the internal changes in the bilayers, we may assume that the chains of the gradient copolymer have several contact points with the hydrophobic and hydrophilic parts of the DPPC membrane in order to minimize their free energy. The hydrophobic monomers would mostly be in contact with the membrane interior and the hydrophilic ones would contact the hydrophilic exterior (Scheme 3). This way their gradient architecture allows them to modify the overall size and lamellarity of DPPC liposomes.

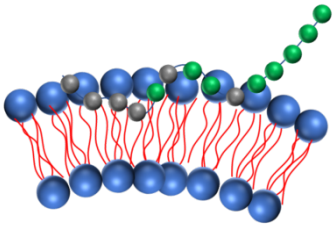

Scheme 3. Schematic representation of DPPC liposome membrane with an incorporated MPOx chain. Lipid heads (blue), lipid tails (red), hydrophilic monomers (green) and hydrophobic monomers (gray) are shown.

First of all, it has to be established that the SLD contrast profiles from SANS are extracted in absolute scale. To that end solvent contrast variation experiments were

performed (Supplementary Material) and it was proved that the fitted SANS profiles could be reproduced by just changing the value of the solvent SLD based on the D_2O/H_2O volume fractions. This fact also supports that there is no measurable contribution from lateral heterogeneities in the formed membranes. In case they existed, their relative intensity would depend on solvent contrast and SANS profiles would not be reproduced [53].

The optimal values of ρ_h and ρ_t were the same in all cases and in agreement with a bilayer fully occupied by DPPC phospholipids and it can be safely assumed that the volume within the bilayer membranes contains negligible amount of water. Based on this the total mass concentration of vesicles in solution c_{SANS} can be extracted (Supplementary Material). As our SANS data do not have well-defined oscillating features at high q our model is not able to distinguish between contributions of different species within the bilayer and apparently provides a coarse-grained average SLD profile. Nevertheless, any change in the apparent mass of the vesicles can be connected to the presence of polymer.

Table 4. Total mass concentration extracted by SANS i.e. c_{SANS} in mgml^{-1} (uncertainty in c_{SANS} ~0.5%).

T (°C)	25			37			45		
c (mgml^{-1})	3	10	30	3	10	30	3	10	30
DPPC	2.01	7.32	23. 1	1.10	5.22	21.1	1.10	4.71	15.0
DPPC-MPOx1	2.51	8.02	22.1	2.50	7.92	22.1	3.31	11.0	27.1
DPPC-MPOx2	4.21	14.0	40.1	4.31	17.1	48.1	1.81	12.0	38.1

Concentration c_{SANS} is compared to the nominal concentration of the preparation protocol (Table~~s 1-3~~4). For DPPC c_{SANS} is lower than the nominal concentration in all cases showing that maybe there is some loss of material during preparation e.g. sticking

to the glass surface. At temperatures higher than 25 ºC more material appears to separate from solution showing a compromise on the stability of liposomes. In DPPC-MPOx1 the situation appears similar at room temperature although there is a somewhat higher c_{SANS} at 3 and 10 mgml^{-1} nominal concentration. This is related to the incorporation of MPOx in the vesicles and the higher efficiency of extracting material from the thin layer to the solution. Interestingly, the vesicular mass is stable at higher temperatures in contrast to the pure DPPC vesicles. The gradient copolymers stabilize the DPPC lipid bilayers, as indicated in our previous studies. Moreover, there is an increase in c_{SANS} at 45 ºC which is in accordance to the increase of the hydrated layer thickness discussed above. This shows that the hydrophobic interaction between DPPC and MPOx becomes stronger and more MPOx enters the bilayer interface. The situation is qualitatively different for MPOx2. Concentration c_{SANS} is systematically higher than the nominal concentration (except from 3 mgml^{-1} at 45 ºC) for DPPC-MPOx2 (Table ~~5~~4). This shows clearly that MPOx2 interacts strongly with DPPC and is incorporated in the bilayers. There is an increase of the hydrophobic interaction from 25 to 37 ºC. Some loss of material results to a decrease of vesicular mass from 37 to 45 ºC and this is significant for nominal concentration 3 mgml^{-1}. Hence, the stronger interaction of MPOx2 in comparison to MPOx1 which is based on the lower number of hydrophilic monomers in MPOx2 is also confirmed by the apparent mass of the mixed vesicles.

4. Conclusions

The effect of MPOx amphiphilic gradient copolymers on DPPC liposomes has been investigated by SANS. The optimal model for data analysis was based on a combination of multi-lamellar vesicles and was adequate to fit all SANS profiles at different concentrations, temperatures and compositions. At room temperature, the copolymer with lower relative hydrophobic content (MPOx1) induced changes in the size of the

bilayer thickness and radius but did not alter the lamellarity combination i.e. uni- and bi-lamellar of DPPC. On the other hand, MPOx2 changes the lamellarity by introducing hexa-lamellar vesicles that are evident by SANS Bragg peaks at the high q regime. At intermediate temperature only uni-lamellar vesicles in DPPC-MPOx1 and DPPC-MPOx2 are present in contrast to pure DPPC. At high temperature lamellarity appears to be concentration dependent in the presence of MPOx2. The use of the certain SANS modelling approach can be useful for analysis of other liposomal systems and their applications as thermoresponsive nanocarriers.

5. Acknowledgmements

This work is based upon experiments performed at the KWS-2 instrument operated by JCNS at the Heinz Maier-Leibnitz Zentrum (MLZ), Garching, Germany.

6. References

[1] M. Salim, H. Minamikawa, A. Sugimura, R. Hashim, Amphiphilic designer nano-carriers for controlled release: from drug delivery to diagnostics, MedChemComm, 5 (2014) 1602-1618.

[2] V.P. Torchilin, Recent advances with liposomes as pharmaceutical carriers, Nature Reviews Drug Discovery, 4 (2005) 145-160.

[3] G. Bozzuto, A. Molinari, Liposomes as nanomedical devices, Int J Nanomedicine, 10 (2015) 975-999.

[4] V. Nele, M.N. Holme, U. Kauscher, M.R. Thomas, J.J. Doutch, M.M. Stevens, Effect of Formulation Method, Lipid Composition, and PEGylation on Vesicle Lamellarity: A Small-Angle Neutron Scattering Study, Langmuir, 35 (2019) 6064-6074.

[5] L.O. De Serrano, D.J. Burkhart, Liposomal vaccine formulations as prophylactic agents: design considerations for modern vaccines, Journal of Nanobiotechnology, 15 (2017) 83.

[6] C.E. Cornell, R.A. Black, M. Xue, H.E. Litz, A. Ramsay, M. Gordon, A. Mileant, Z.R. Cohen, J.A. Williams, K.K. Lee, G.P. Drobny, S.L. Keller, Prebiotic amino acids bind to and stabilize prebiotic fatty acid membranes, Proceedings of the National Academy of Sciences, 116 (2019) 17239-17244.

[7] T.F. Zhu, J.W. Szostak, Coupled growth and division of model protocell membranes, J Am Chem Soc, 131 (2009) 5705-5713.

[8] N.J. Zuidam, D. Hirsch-Lerner, S. Margulies, Y. Barenholz, Lamellarity of cationic liposomes and mode of preparation of lipoplexes affect transfection efficiency, Biochimica et Biophysica Acta (BBA) - Biomembranes, 1419 (1999) 207-220.

[9] P. Pucci, A. Scipioni, C. La Mesa, Albumin binding onto synthetic vesicles, Soft Matter, 8 (2012) 9669–9675.

[10] F. Ruggeri, F. Zhang, T. Lind, E.D. Bruce, B.L.T. Lau, M. Cárdenas, Non-specific interactions between soluble proteins and lipids induce irreversible changes in the properties of lipid bilayers, Soft Matter, 9 (2013) 4219-4226.

[11] A. Papagiannopoulos, Bovine serum albumin interactions with cationic surfactant vesicles decorated by a low-molar-mass polysaccharide, Colloids and Surfaces A: Physicochemical and Engineering Aspects, 537 (2018) 495-501.

[12] L. Paasonen, B. Romberg, G. Storm, M. Yliperttula, A. Urtti, W.E. Hennink, Temperature-Sensitive Poly(N-(2-hydroxypropyl)methacrylamide mono/dilactate)-Coated Liposomes for Triggered Contents Release, Bioconjugate Chemistry, 18 (2007) 2131-2136.

[13] N. Pippa, A. Meristoudi, S. Pispas, C. Demetzos, Temperature-dependent drug release from DPPC:C12H25-PNIPAM-COOH liposomes: Control of the drug loading/release by modulation of the nanocarriers' components, International Journal of Pharmaceutics, 485 (2015) 374-382.

[14] G.A.T. Kaminski, M.R. Sierakowski, R. Pontarolo, L.A.d. Santos, R.A.d. Freitas, Layer-by-layer polysaccharide-coated liposomes for sustained delivery of epidermal growth factor, Carbohydrate Polymers, 140 (2016) 129-135.

[15] M.-T. Popescu, S. Mourtas, G. Pampalakis, S.G. Antimisiaris, C. Tsitsilianis, pH-Responsive Hydrogel/Liposome Soft Nanocomposites For Tuning Drug Release, Biomacromolecules, 12 (2011) 3023-3030.

[16] T.P.T. Dao, A. Brûlet, F. Fernandes, M. Er-Rafik, K. Ferji, R. Schweins, J.P. Chapel, A. Fedorov, M. Schmutz, M. Prieto, O. Sandre, J.F. Le Meins, Mixing Block Copolymers with Phospholipids at the Nanoscale: From Hybrid Polymer/Lipid Wormlike Micelles to Vesicles Presenting Lipid Nanodomains, Langmuir, 33 (2017) 1705-1715.

[17] F.A. Heberle, R.S. Petruzielo, J. Pan, P. Drazba, N. Kučerka, R.F. Standaert, G.W. Feigenson, J. Katsaras, Bilayer Thickness Mismatch Controls Domain Size in Model Membranes, J Am Chem Soc, 135 (2013) 6853-6859.

[18] A. Grau-Campistany, E. Strandberg, P. Wadhwani, J. Reichert, J. Bürck, F. Rabanal, A.S. Ulrich, Hydrophobic mismatch demonstrated for membranolytic peptides and their use as molecular rulers to measure bilayer thickness in native cells, Scientific Reports, 5 (2015) 9388.

[19] E. Vlassi, A. Papagiannopoulos, S. Pispas, Amphiphilic poly(2-oxazoline) copolymers as self-assembled carriers for drug delivery applications, European Polymer Journal, 88 (2017) 516-523.

[20] G. Hochleitner, J.F. Hümmer, R. Luxenhofer, J. Groll, High definition fibrous poly(2-ethyl-2-oxazoline) scaffolds through melt electrospinning writing, Polymer, 55 (2014) 5017-5023.

[21] T.X. Viegas, M.D. Bentley, J.M. Harris, Z. Fang, K. Yoon, B. Dizman, R. Weimer, A. Mero, G. Pasut, F.M. Veronese, Polyoxazoline: Chemistry, Properties, and Applications in Drug Delivery, Bioconjugate Chemistry, 22 (2011) 976-986.

[22] Z. He, L. Miao, R. Jordan, D. S-Manickam, R. Luxenhofer, A.V. Kabanov, A Low Protein Binding Cationic Poly(2-oxazoline) as Non-Viral Vector, Macromolecular Bioscience, 15 (2015) 1004-1020.

[23] N. Pippa, A. Dokoumetzidis, S. Pispas, C. Demetzos, The interplay between the rate of release from polymer grafted liposomes and their fractal morphology, International Journal of Pharmaceutics, 465 (2014) 63-69.

[24] N. Pippa, M. Merkouraki, S. Pispas, C. Demetzos, DPPC:MPOx chimeric advanced Drug Delivery nano Systems (chi-aDDnSs): Physicochemical and structural characterization, stability and drug release studies, International Journal of Pharmaceutics, 450 (2013) 1-10.

[25] J. Drazenovic, H. Wang, K. Roth, J. Zhang, S. Ahmed, Y. Chen, G. Bothun, S.L. Wunder, Effect of lamellarity and size on calorimetric phase transitions in single component phosphatidylcholine vesicles, Biochimica et Biophysica Acta (BBA) - Biomembranes, 1848 (2015) 532-543.

[26] A. Papagiannopoulos, Chapter 10 - Small-Angle Neutron Scattering (SANS), in: S. Thomas, R. Thomas, A.K. Zachariah, R.K. Mishra (Eds.) Microscopy Methods in Nanomaterials Characterization, Elsevier, 2017, pp. 339-361.

[27] E. Di Cola, I. Grillo, S. Ristori, Small Angle X-ray and Neutron Scattering: Powerful Tools for Studying the Structure of Drug-Loaded Liposomes, Pharmaceutics, 8 (2016) 10.

[28] L. Arleth, C. Vermehren, An analytical model for the small-angle scattering of polyethylene glycol-modified liposomes, Journal of Applied Crystallography, 43 (2010) 1084-1091.

[29] Y. Milonaki, E. Kaditi, S. Pispas, C. Demetzos, Amphiphilic gradient copolymers of 2-methyl- and 2-phenyl-2-oxazoline: self-organization in aqueous media and drug encapsulation, Journal of Polymer Science Part A: Polymer Chemistry, 50 (2012) 1226-1237.

[30] J.G. Barker, J.S. Pedersen, Instrumental Smearing Effects in Radially Symmetric Small-Angle Neutron Scattering by Numerical and Analytical Methods, Journal of Applied Crystallography, 28 (1995) 105-114.

[31] A. Radulescu, N.K. Szekely, S. Polachowski, M. Leyendecker, M. Amann, J. Buitenhuis, M. Drochner, R. Engels, R. Hanslik, G. Kemmerling, P. Lindner, A. Papagiannopoulos, V. Pipich, L. Willner, H. Frielinghaus, D. Richter, Tuning the instrument resolution using chopper and time of flight at the small-angle neutron scattering diffractometer KWS-2, Journal of Applied Crystallography, 48 (2015) 1849-1859.

[32] T. Vad, W.F.C. Sager, J. Zhang, J. Buitenhuis, A. Radulescu, Experimental determination of resolution function parameters from small-angle neutron scattering data of a colloidal SiO2 dispersion, Journal of Applied Crystallography, 43 (2010) 686-692.

[33] A. Papagiannopoulos, A. Meristoudi, S. Pispas, A. Radulescu, Micelles from HOOC-PnBA-b-PAA-C12H15 Diblock Amphiphilic Polyelectrolytes as Protein Nanocarriers, Biomacromolecules, 17 (2016) 3816–3827.

[34] D. Vanderbilt, S.G. Louie, A Monte carlo simulated annealing approach to optimization over continuous variables, Journal of Computational Physics, 56 (1984) 259-271.

[35] H. Frielinghaus, Small-angle scattering model for multilamellar vesicles, Physical Review E, 76 (2007) 051603.

[36] H. Iatrou, H. Frielinghaus, S. Hanski, N. Ferderigos, J. Ruokolainen, O. Ikkala, D. Richter, J. Mays, N. Hadjichristidis, Architecturally Induced Multiresponsive Vesicles from Well-Defined Polypeptides. Formation of Gene Vehicles, Biomacromolecules, 8 (2007) 2173-2181.

[37] A. Papagiannopoulos, J. Zhao, G. Zhang, S. Pispas, A. Radulescu, Thermoresponsive transition of a PEO-b-PNIPAM copolymer: From hierarchical aggregates to well defined ellipsoidal vesicles, Polymer, 54 (2013) 6373-6380.

[38] D. Uhríková, N. Kučerka, J. Teixeira, V. Gordeliy, P. Balgavý, Structural changes in dipalmitoylphosphatidylcholine bilayer promoted by Ca2+ ions: a small-angle neutron scattering study, Chemistry and Physics of Lipids, 155 (2008) 80-89.

[39] K. Komorowski, A. Salditt, Y. Xu, H. Yavuz, M. Brennich, R. Jahn, T. Salditt, Vesicle Adhesion and Fusion Studied by Small-Angle X-Ray Scattering, Biophys J, 114 (2018) 1908-1920.

[40] N. Kučerka, J.F. Nagle, S.E. Feller, P. Balgavý, Models to analyze small-angle neutron scattering from unilamellar lipid vesicles, Physical Review E, 69 (2004) 051903.

[41] H. JS, B. HC., Polymers and neutron scattering, OUP, 1994.

[42] J.S. Pedersen, Analysis of small-angle scattering data from colloids and polymer solutions: modeling and least-squares fitting, Advances in Colloid and Interface Science, 70 (1997) 171-210.

[43] K. Stovgaard, C. Andreetta, J. Ferkinghoff-Borg, T. Hamelryck, Calculation of accurate small angle X-ray scattering curves from coarse-grained protein models, BMC Bioinformatics, 11 (2010) 429-429.

[44] A. Koutsioubas, Combined Coarse-Grained Molecular Dynamics and Neutron Reflectivity Characterization of Supported Lipid Membranes, The Journal of Physical Chemistry B, 120 (2016) 11474-11483.

[45] M. Belička, Y. Gerelli, N. Kučerka, G. Fragneto, The component group structure of DPPC bilayers obtained by specular neutron reflectometry, Soft Matter, 11 (2015) 6275-6283.

[46] J.F. Nagle, S. Tristram-Nagle, Structure of lipid bilayers, Biochim Biophys Acta, 1469 (2000) 159-195.

[47] M. Hirai, H. Iwase, T. Hayakawa, M. Koizumi, H. Takahashi, Determination of asymmetric structure of ganglioside-DPPC mixed vesicle using SANS, SAXS, and DLS, Biophys J, 85 (2003) 1600-1610.

[48] S.J. Marrink, J. Risselada, A.E. Mark, Simulation of gel phase formation and melting in lipid bilayers using a coarse grained model, Chemistry and Physics of Lipids, 135 (2005) 223-244.

[49] J. Gallová, D. Uhríková, N. Kučerka, S. Doktorovová, S.S. Funari, J. Teixeira, P. Balgavý, The effects of cholesterol and β-sitosterol on the structure of saturated diacylphosphatidylcholine bilayers, European Biophysics Journal, 40 (2011) 153-163.

[50] N. Pippa, E. Kaditi, S. Pispas, C. Demetzos, DPPC/poly(2-methyl-2-oxazoline)-grad-poly(2-phenyl-2-oxazoline) chimeric nanostructures as potential drug nanocarriers, Journal of Nanoparticle Research, 15 (2013) 1685.

[51] J.-H. Lee, V. Agarwal, A. Bose, G.F. Payne, S.R. Raghavan, Transition from Unilamellar to Bilamellar Vesicles Induced by an Amphiphilic Biopolymer, Physical Review Letters, 96 (2006) 048102.

[52] B.-S. Yang, J. Lal, P. Richetti, C.M. Marques, W.B. Russel, R.K. Prud'homme, Interaction of Hydrophobically Modified Polymers and Surfactant Lamellar Phase, Langmuir, 17 (2001) 5834-5841.

[53] F.A. Heberle, V.N.P. Anghel, J. Katsaras, Scattering from phase-separated vesicles. I. An analytical form factor for multiple static domains, Journal of Applied Crystallography, 48 (2015) 1391-1404.